Ca$_{1-x-y}$Yb$_x$Pr$_y$F$_{2+x+y}$ solid solution powders as a promising materials for crystalline silicon solar energetics

S. V. Kuznetsov[1], O. A. Morozov[2], V. G. Gorieva[2], M. N. Mayakova[1], M. A. Marisov[2], V. V. Voronov[1],
A. D. Yapryntsev[3], V. K. Ivanov[3], E. I. Madirov[2], A. S. Nizamutdinov[2], V. V. Semashko[2], P. P. Fedorov[1]

[1]Prokhorov General Physics Institute, RAS, 38 Vavilova str., Moscow, 119991 Russia

[2]Kazan Federal University, 18 Kremljovskaya, Kazan, 420008 Russia

[3]Kurnakov Institute of General and Inorganic Chemistry, RAS, 31 Leninsky pr., Moscow,119991 Russia

kouznetzovsv@gmail.com

We have synthesized single-phase powders of Ca$_{1-x-y}$Yb$_x$Pr$_y$F$_{2+x+y}$ solid solutions with an average particle size of about 35 nm by co-precipitation from aqueous nitrate solutions. After annealing at 600 °C during 1 hour, the particle size was increased up to 150–200 nm. Individual luminescence bands of praseodymium are distinguishable in the luminescence spectrum. The intensity of the luminescence of ytterbium increased by a factor of 1000 in comparison with the unannealed samples. The highest luminescence intensity of ytterbium was detected for the Ca$_{0.9495}$Yb$_{0.0500}$Pr$_{0.0005}$F$_{2.0505}$.

1. Introduction

Solar energy is one of the most abundant energy sources [1, 2] and crystalline silicon solar panels became a quite traditional tool for its utilization. The use of silicon has its major advantage in its chemical availability, as well as well-developed manufacturing and recycling technology, including recycling of the rare-earth-containing components. Other solar panels, such as GaAs, CdTe, Cu(In,Ga)Se$_2$ multiple layer devices, can also be utilized for the solar energy conversion [1], but their manufacturing and recycling is more complicated and expensive due to their toxicity. In other words, the use of GaAs, CdTe, and/or Cu(In,Ga)Se$_2$ doesn't obey "green chemistry" principles. Unfortunately, silicon solar panels possess relatively low coefficients for converting solar power to electric energy (under 25 % even for the best samples [1, 2]). This is why silicon solar cells are frequently modified by luminescent coatings. These phosphor films can transform solar energy from the spectral region of photon nonsusceptibility (ultra-violet and visible range) of crystalline silicon solar cells to the region of their photoresponse (infra-red range).

Down-conversion luminescence, especially quantum cutting mechanism is one of the promising pathways of increasing crystalline silicon solar cell efficiency [1, 3]. Quantum cutting allows for splitting each energy UV photon to two infra-red photons [4]. When Pr is excited at a wavelength of 185 nm, a quantum conversion efficiency of more than 100 % was obtained.

Later publications concerning down-conversion phenomenon also demonstrated quantum yields of more than 100 % for several materials [1].

Fluorite-type solid solutions M$_{1-x}$R$_x$F$_{2+x}$ (M = Ca, Sr, Ba, R – rare earth) exists in all MF$_2$-RF$_3$ systems [5]. Single-phase solid solutions in the systems Ca$_{1-x}$R$_x$F$_{2+x}$ are formed up to x = 0.2 [6], Sr$_{1-x}$R$_x$F$_{2+x}$ x = 0.6 [7]. For systems based on BaF$_2$-RF$_3$, single-phase solid solutions with low dopant content cannot be synthesized [8–10]. Effective up- and down-conversion luminescence is carried out through the interaction of the cations introduced in the matrix. Calcium fluoride matrix possesses certain technological advantages, for it has crystal lattice parameters close to that of silicon, so CaF$_2$-based films can easier be attached to silicon substrates by epitaxy [11–13].

Thus it is of great interest to study CaF$_2$ matrix with Pr^{3+}-Yb^{3+} ions pair doped due to the existence of resonant transitions ^{3}P$_0$−^{1}G$_4$ of Pr^{3+} and ^{2}F$_{7/2}$ – ^{2}F$_{5/2}$-transitions of Yb^{3+} ions [14] which is promising for quantum cutting by means of energy transfer from Pr^{3+} ions to Yb^{3+} ions. Therefore, the goal of the present study was the investigation of chemical and physical properties of Ca$_{1-x-y}$Yb$_x$Pr$_y$F$_{2+x+y}$ solid solutions for determining the chemical compositions suitable for increasing the efficiency of crystalline silicon solar panels.

2. Experimental

We used 99.99 wt% pure ytterbium and praseodymium nitrate hexahydrates, calcium nitrate tetrahydrate (all reagents were manufactured by LANHIT, Russia), 99.99 wt% pure 46–49 wt% aqueous hydrogen fluoride (SigmaTec, Russia) and double distilled water as the starting materials, without further purification. Fluorite-type CaF_2:Yb:Pr solid solution precipitates were synthesized according to our previously published protocol [15]. 0.5 M calcium, praseodymium, ytterbium nitrate aqueous solutions were added dropwise to the two-fold excess of 5.0 M aqueous HF under vigorous magnetic stirring. The process of co-precipitation is based on the fact that the solubility of alkaline-earth and rare-earth fluorides in water is low (about 10^{-5}-10^{-4} M) [16,17]. After CaF_2:Yb:Pr precipitate was formed, the mother solution was decanted. Precipitates formed were washed with double distilled water until negative nitrate anion test with diphenylamine. This qualitative reaction is based on the oxidation of diphenylamine, which has a sensitivity to nitrate ions. Colorless diphenyl benzidine is first formed, which upon further oxidation is converted into a diphenyl benzidine quinoid derivative having a blue color. Obtained powders were dried in air at 45 °C for 5 hours and annealed in platinum crucibles (also in air) at 600 °C for 1 hour.

All samples were analyzed using a Bruker D8 Advanced (Cu Kα radiation) diffractometer. Particle sizes and morphology were determined by a Carl Zeiss NVision 40 scanning electron microscope. Differential thermal analysis (DTA) and differential thermal gravimetric analysis (DTG) was performed on a MOM Q-1500 D derivatograph with platinum crucible on air (rate of heating/cooling - 10 degrees/min). Fluorescence of the samples was excited by a 443 nm cw laser diode with a pumping power density of 152.8 W/cm^2. The luminescence spectra were recorded with Stellarnet EPP 2000 spectrometer using a 5 mm filter (ZhS-16) and corrected for the spectral sensitivity of spectrometer. The luminescence kinetics were registered with the use of scanning monochromator with 600 l/mm diffraction grating and under pulsed excitation with 444 nm laser light from OPO system Lotis TII LT2211. The luminescence light was converted by photomultiplier tube FEU62 and digitalized by BORDO oscilloscope.

3. Results

Typical X-ray diffraction pattern of CaF_2:Yb:Pr unannealing sample is presented in Fig. 1a. All observed reflections are in a good agreement with JCPDS Card #77-2245 data, i.e., XRD results confirmed that synthesized samples contain only one fluorite-type phase. According to our previous experimental data for similar samples, the luminescence intensity of unannealed samples was low. One of the main reasons for this is the presence of hydroxyl anions in the crystal lattice, which result in quenching of luminescence. We chose the annealing temperature based on DTA/DTG study (Fig. 2). It's clear, that the dehydration proceeds in several stages and finishes at about 500–550 °C. Weight loss upon was 3.7 wt%. Based on this we chose the 600 °C and 1 hour as annealing conditions. Fig. 1b represents XRD data for annealed sample. Lines in the X-ray pattern of the sample dried at 45 °C (Fig. 1a), were much broader than the lines for the sample annealed at 600 °C (Fig. 1b). Annealing leads to an increased crystallite size. We calculated the unit cell parameters for the samples before and after annealing (Table 1). Annealing at 600 °C resulted in an anticipated small decrease in the unit cell parameter value in comparison with the data for the same composition samples dried at 45 °C: see also [18] for the similar dehydration effect studies. The weight loss upon for dehydration in Table 1 and in TG data in DTA/DTG study were similar.

Typical scanning electron microscopy (SEM) images of the samples dried at 45 °C are presented in Fig. 3a,b,c. SEM results confirm that particle sizes vary from 20 nm to 80 nm (average particle size is about 35 nm). Fig. 3b presents SEM image taken in EBSD regime, which allow for atomic contrast regime. The uniform color of the image on Fig. 3b confirms the single phase composition of the powders. Annealing at 600 °C caused the increase in the particle sizes up to $\sim$150–200 nm (Fig. 3d,e). Evaluation of chemical composition based on EDX analysis is summarized in Table 2. The content of praseodymium in the solid solutions is close to it's nominal content in initial aqueous solution. The content of ytterbium fluoride in solid solutions is somewhat higher than in aqueous solution. The EDX composition determination error is 0.5 mol.%. This means that the concentration of praseodymium in the samples may also be greater than in the case of ytterbium. The mean value of ytterbium distribution coefficient between solid and aqueous phases is about 1.45. This means that the crystallization proceeds in an incongruent manner.

Characteristic luminescence spectra of the samples before and after annealing are presented in Fig. 4a. The luminescence intensity of the unannealed sample appeared to be very low as it has been predicted and intensity of Yb^{3+} luminescence at the wavelengths around 1 micrometer was almost at the level of noise. In the visible spectral range, we have registered broad luminescence band located in the region of praseodymium luminescence. After annealing/dehydration stage, the luminescence spectra have changed. In the visible spectral range, characteristic
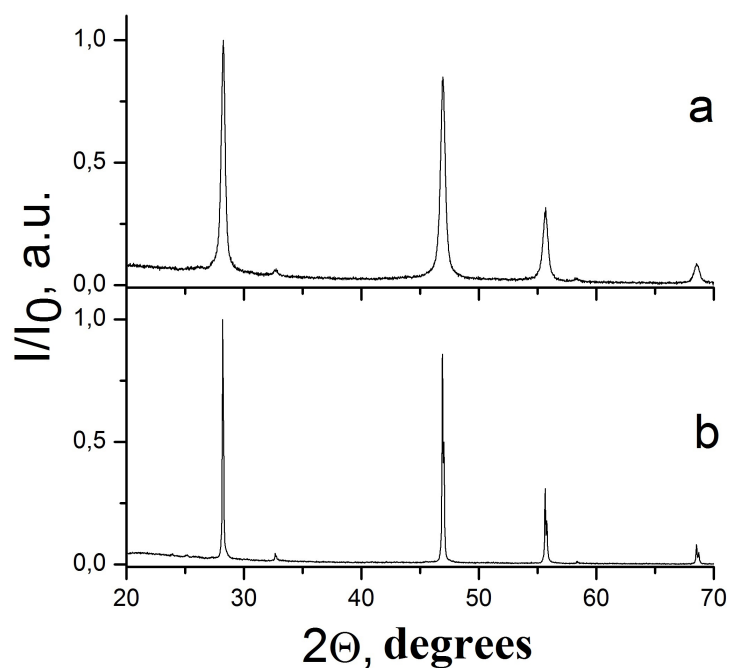
FIG. 1. XRD patterns of CaF$_2$:Yb (5.0mol%):Pr (0.1 mol%) powder: dried at 45 °C (a), and annealed at 600 °C (b)

TABLE 1. XRD results for CaF$_2$:Yb:Pr solid solutions

No*	Nominal doping Pr/Yb, mol. %	After drying at 45 °C	After annealing at 600 °C	Weight loss upon, wt.%
		a, Å	a, Å	
1	0.01/7.0	5.4757(7)	5.4700(6)	4.5
2	0.01/10.0	5.463(2)	5.460(3)	3.8
3	0.01/12.0	5.4799(4)	5.4774(4)	4.2
4	0.05/5.0	5.461(2)	5.464(1)	4.3
5	0.05/7.0	5.476(1)	5.4694(7)	4.1
6	0.05/10	5.4741(8)	5.47643(8)	4.7
7	0.05/12.0	5.4757(7)	5.472(1)	4.1
8	0.05/20.0	5.4826(7)	5.4850(8)	4.8
9	0.1/1	5.460(2)	5.4627(2)	5.7
10	0,1/5	5.4747(3)	5.4737(6)	5.6
11	0.1/10	5.490(2)	5.4759(4)	5.5
12	0.1/20	5.4802(9)	5.481(1)	4.9
13	1/5	5.475(1)	5.469(1)	5.6
14	1/10	5.4731(5)	5.4804(3)	2.7

* – The sample labeling used in Table 1 is maintained across
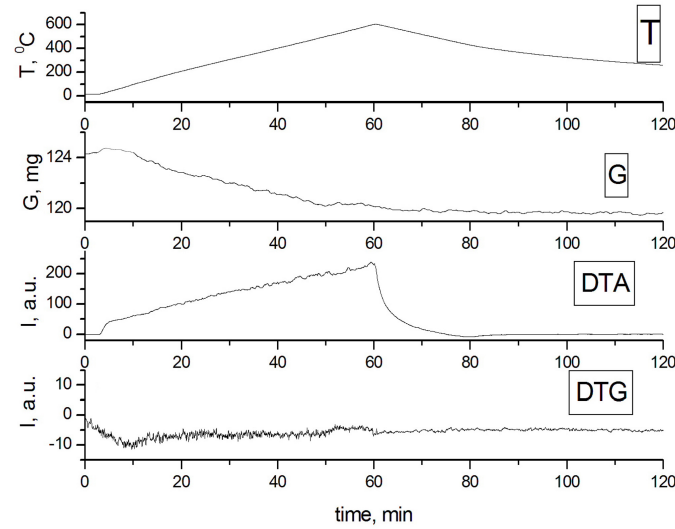the whole paper for the reader's convenience.

FIG. 2. DTA/DTG analysis of CaF_2:Yb(7.0 mol.%):Pr(0.01 mol.%) precipitate. T – temperature, G – weight, DTA – differential thermal analysis, DTG – differential thermal gravimetry. The weights at annealing was 3.7 wt.%

TABLE 2. EDX results for CaF_2:Yb:Pr samples

Sample number – temperature of drying	Pr/Yb, mol.%		The effective praseodymium/ytterbium distribution coefficient
	Nominal doping	Doping based on EDX	
10–45	0.1/5.0	*/6.8	–/1.36
10–600	0.1/10.0	*/7.1	–/1.42
11–600	0.1/10.0	*/15.5	–/1.55
13–45	1.0/5.0	1.1/7.9	1.1/1.58
14–45	1.0/10.0	1.1/14.9	1.1/1.49

* The content of praseodymium is below the limit of reliable determination.

spectral lines of praseodymium ions have been resolved which agree with literature data [19] and consistent with data for other fluoride systems containing Pr^{3+} [20–22]. These lines correspond to numerous transitions from ^3P_J manifold to ^3H_J and ^3F_J manifolds. The intensity of ytterbium luminescence at around 1-micrometer spectral range has increased one thousand fold. It means that annealing stage is an efficient tool for dehydration and increasing of ytterbium luminescence.

Luminescence spectra for series of annealed samples with different Pr^{3+} and Yb^{3+} ions content have been investigated. Characteristic spectra are presented in Fig. 4b. The inset shows luminescence lines in visible spectral range in enlarged intensity scale. The known Pr^{3+} ion luminescence lines are registered in the visible spectral range. The intense luminescence within 900–1100 nm range corresponding to $^2F_{5/2}-^2F_{7/2}$ transitions of Yb^{3+} ions was detected. This indicates a successful transfer of excitation energy from praseodymium to ytterbium. Intense luminescence of ytterbium at $\lambda = 1$ μm overlaps the photosensitivity region of crystalline silicon solar cells [1, 3]. We observe a decrease of Pr^{3+} luminescence intensity with higher Yb^{3+} content for samples with low levels of Pr^{3+} doping which proves down-conversion approach for the selected ions pair. This also indicates the applicability of this approach to increase the efficiency of solar cells. At the same time, the decrease of shorter wavelength peak of Yb^{3+} luminescence is observed with the increase of Yb^{3+} content, which speaks about reabsorption process.

Unfortunately, the effort to increase the down-conversion yield by an increase of Pr^{3+} ion content does not yield positive results. In Fig. 5a one can see that luminescence lines intensity of Pr^{3+} ions increase while the
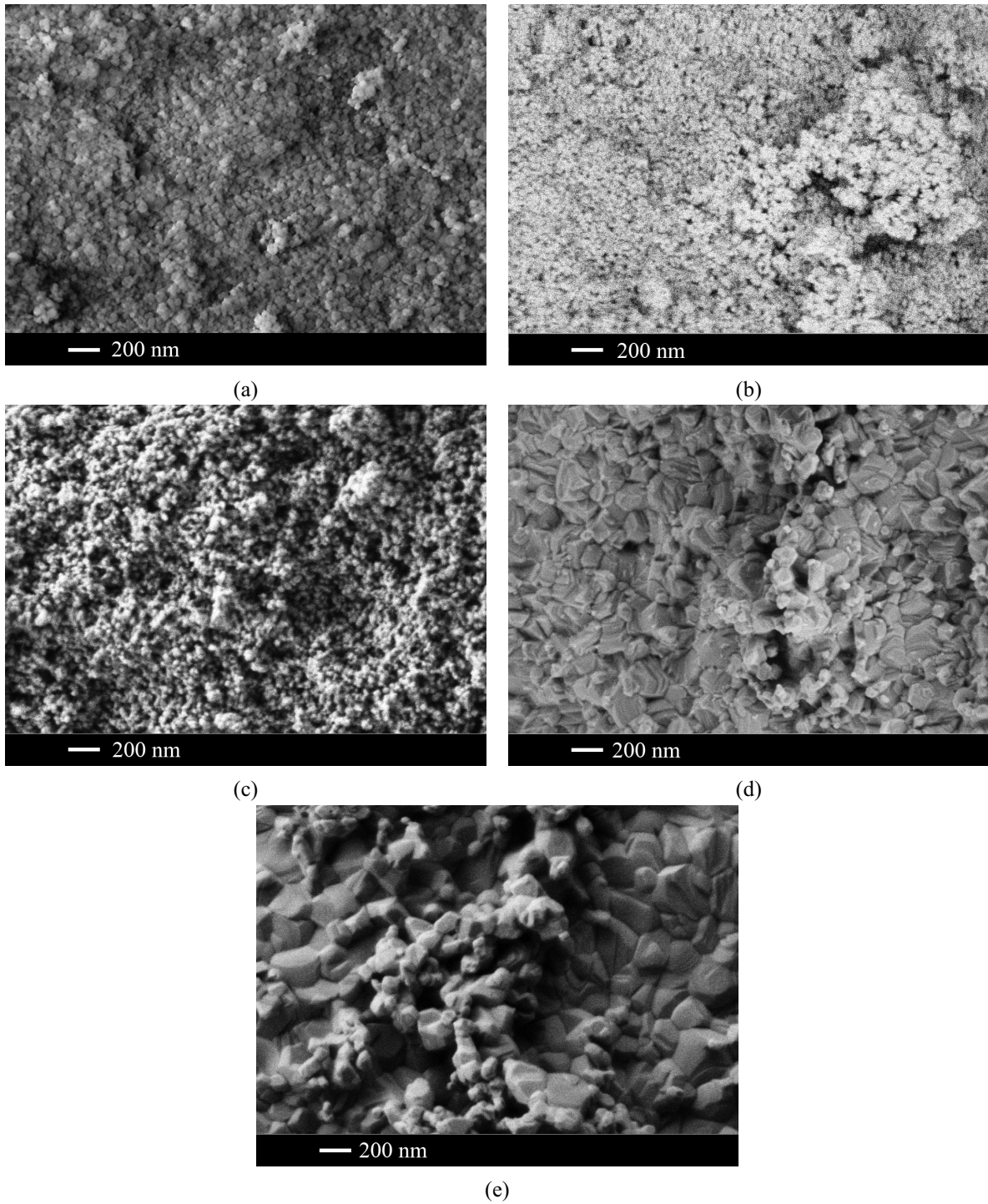
FIG. 3. (a) SEM image of sample 10 after drying at 45 °C. (b) SEM image (EBSD regime) of sample 13 after drying at 45 °C. (c) SEM image of sample 14 after drying at 45 °C. (d) SEM image of sample 10 after annealing at 600 °C. (e) SEM image of sample 11 after annealing at 600 °C.
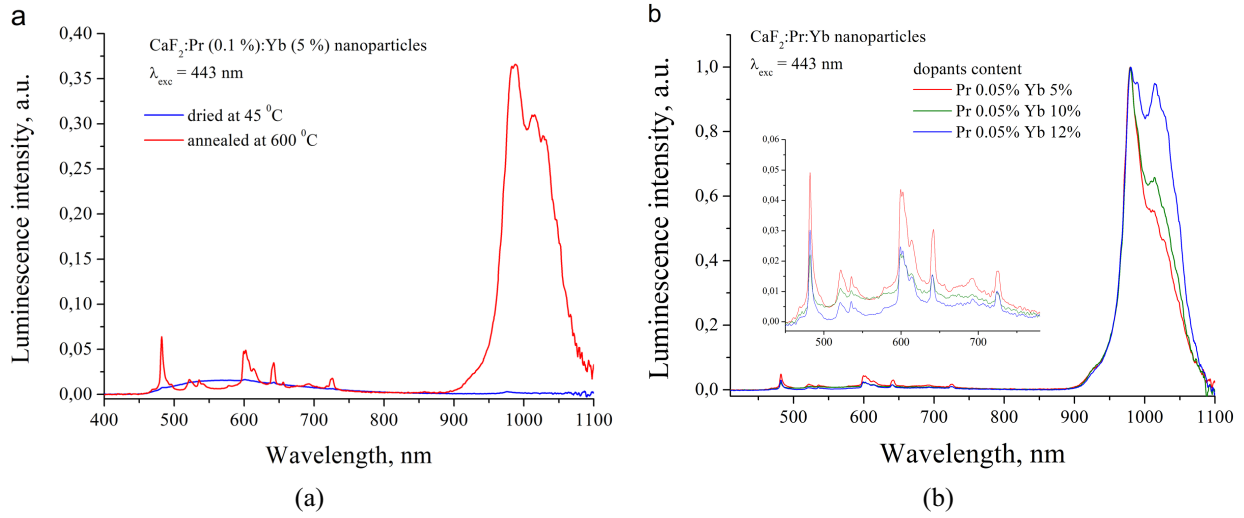
FIG. 4. Luminescence spectra for sample of CaF_2 with Pr^{3+} (0.1 %) and Yb (5 %) before and after annealing (a), luminescence of a series of CaF_2:Pr:Yb samples annealed at 600 °C (b)

intensity of Yb^{3+} ions drops for samples with 5 % of Yb^{3+} when increasing the Pr^{3+} content from 0.05 % to 1 %. Apparently, we have the opposing process of radiationless decay of Yb^{3+} ions excited state.

In order to clarify this, we have studied the Yb^{3+} luminescence decay kinetics in the series of samples with constant Yb^{3+} content and varying Pr^{3+} content. In the Fig. 5b luminescence decay curves of Yb^{3+} detected at 978 nm are presented. It is clearly seen that Yb^{3+} luminescence lifetime drops with increased Pr^{3+} ion content.
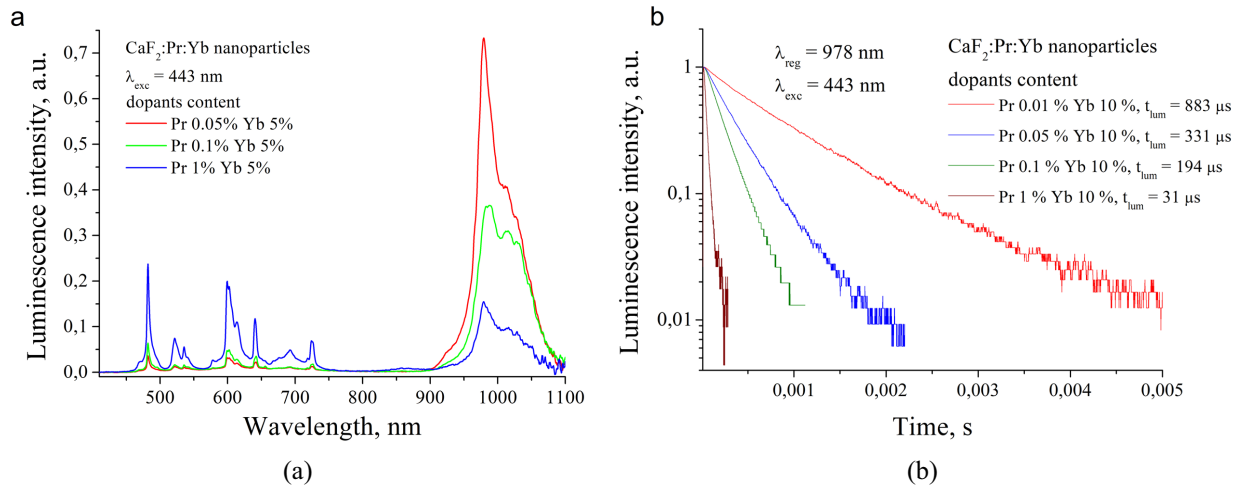

FIG. 5. Luminescence spectra (a) and Yb^{3+} luminescence decay (b) for samples of CaF_2 with constant Yb^{3+} content (10 %) and various Pr^{3+} content

Apparently, this quenching occurs due to close location of $^2F_{5/2}$ and $^1G_4$ manifolds for Yb^{3+} and Pr^{3+} ions respectively in the band gap of CaF_2 matrix which provides energy transfer from Yb^{3+} to Pr^{3+} ions. This process brings more restrictions to search for optimal Yb and Pr ions composition in CaF_2 for means of efficient down-conversion. The highest level of luminescence intensity among all the studied samples was observed for the composition CaF_2:Pr (0.05 mol.%):Yb (5.0 mol.%).

4. Conclusions

Single-phase precipitates with an average particle size of about 35 nm were formed upon precipitation of $Ca_{1-x-y}Yb_xPr_yF_{2+x+y}$ solid solutions from the corresponding aqueous nitrate solutions. Crystallization of fluoride phases proceeds according to the incongruent mechanism. The mean value of the ytterbium distribution coefficient

was about 1.45. These samples dried at 45 °C had weak luminescence intensities. The annealing step for dehydration was found to be necessary for intensity luminescence increasing. According to DTA/DTG study, the temperature of annealing must be higher than 550 °C. The annealing conditions chosen for further study were 600 °C, 1 hour. After annealing, the particle size increased up to 150–200 nm. Individual luminescence bands of praseodymium are distinguishable in the luminescence spectrum. The intensity of the luminescence of ytterbium increased by 1000-fold. At the same time, we have observed the quenching of Yb^{3+} ions luminescence at high levels of Pr^{3+} content apparently due to energy transfer from $^2F_{5/2}$ manifold of Yb^{3+} to $^1G_4$ manifold of Pr^{3+} ion. The highest luminescence intensity of ytterbium was determined for a $Ca_{0.9495}Yb_{0.0500}Pr_{0.0005}F_{2.0505}$ solid solution. This composition is substantial interest for further experiments aimed at the creation of luminescent coatings on crystalline silicon designed to increase the efficiency of solar panels.

Acknowledgements

References

[1] Huang X., Han S., Huang W., Liu X. Enhancing solar cell efficiency: the search for luminescent materials as spectral converters. *Chem. Soc. Rev.*, 2013, **42**, P. 173–201.

[2] Green M.A., Bremner S.P. Energy conversion approaches and materials for high-efficiency photovoltaics. *Nature Mater.*, 2017, **16**, P. 23–34.

[3] Richardson B.S. Enhancing the performance of silicon solar cells via the application of passive luminescence conversion layers. *Solar Energy Materials & Solar Cells*, 2006, **90**, P. 2329–2337.

[4] Piper W.W., DeLuca J.A., Ham F.S. Cascade fluorescent decay in Pr^{3+}-doped fluorides: Achievement of a quantum yield greater than unity for emission of visible light. *J. Lumin.*, 1974, **8**, P. 344–348.

[5] Sobolev B.P. *The Rare Earth Trifluorides. Part 1. The High Temperature Chemistry of the Rare Earth Trifluorides*. Institut d'Estudis Catalans, Barcelona, Spain, 2000, 520 pp.

[6] Fedorov P.P., Mayakova M.N., Kuznetsov S.V., et. al. Synthesis of CaF_2-YF_3 nanopowders by co-precipitation from aqueos solutions. *Nanosystems: Physics, Chemistry, Mathematics*, 2017, **8**(4), P. 462–470.

[7] Mayakova M.N., Luginina A.A., Kuznetsov S.V., et. al. Synthesis of SrF_2-YF_3 nanopowders by co-precipitation from aqueous solutions. *Mendeleev Communications*, 2014, **24**(6), P. 360–362.

[8] Kuznetsov S.V., Fedorov P.P., Voronov V.V., et. al. Synthesis of $Ba_4R_3F_{17}$ (R stands for Rare-Earth Elements) Powders and Transparent Compacts on Their Base. *Rus. J. Inorg. Chem.*, 2010, **55**(4), P. 484–493.

[9] Fedorov P.P., Mayakova M.N., Kuznetzov S.V., et. al. Co-precipitation of yttrium and barium fluorides from aqueous solutions. *Materials Research Bulletin*, 2012, **47**, P. 1794–1799.

[10] Karbowiak M., Cichos J. Does $BaYF_5$ nanocrystal exist? – The BF_2-YF_3 solid solution revisited using photoluminescence spectroscopy. *J. Alloy Compd.*, 2016, **673**, P. 258–264.

[11] ElFajri A., Moussetad M., Tardy P., Barriere A.S. Electrical study of Pr^{3+} ion environment in $Ca_{1-x}Pr_xF_{2+x}$ thin films. *Phys. Status solidi (a)*, 2000, **179**, P. 373–386.

[12] Sokolov N.S., Suturin S.M. MBE growth of calcium and cadmium fluoride nanostructures on silicon. *Appl. Surf. Sci.*, 2002, **175–176**, P. 619–628.

[13] Blunier S., Zogg H., Maissen C., et. al. Lattice and thermal misfit dislocation in epitaxial CaF_2/Si(111) and BaF_2-CaF_2/Si(111) structures. *Phys. Rev. Lett.*, 1992, **68**(24), P. 3599–3602.

[14] Yagoub M.Y.A., Swart H.C., Coetsee E. Concentration quenching, surface and spectral analyses of SrF_2:Pr^{3+} prepared by different synthesis techniques. *Opt. Mater.*, 2015, **42**, P. 204–209.

[15] Fedorov P.P., Mayakova M.N., Kuznetsov S.V., Voronov V.V. Low temperature phase formation in the CaF_2–HoF_3 system. *Russ. J. Inorg. Chem.*, 2017, **62**(9), P. 1173–1176.

[16] Batsanova L.R. Rare-earth fluorides. *Rus. Chem. Rev.*, 1971, **40**(6), P. 465–484.

[17] *Gmelin Handbuch der anorganischen Chemie. Syst. Nummer 39: Seltenerdelemente. Teil C.3: Sc, Y, La und Lanthanide. Fluoride, Oxifluoride und zugehogige Alkalidoppelverbindungen*. Berlin, Springer Vlg., 1976, 439 pp.

[18] Rozhnova Yu.A., Kuznetsov S.V., Luginina A.A., et. al., New $Sr_{1-x-y}R_x(NH_4)_yF_{2+x-y}$ (R = Yb, Er) solid solution as precursor for high efficiency up-conversion luminophor and optical ceramics on the base of strontium fluoride. *Mater. Chem. Phys.*, 2016, **172**, P. 150–157.

[19] Dieke G.H., Crosswhite H.M. The spectra of the doubly and triply ionized rare earths. *Appl. Opt.*, 1963, **2**, P. 675–686.

[20] Kuzmanoski A., Pankratov V., Feldmann C. Energy transfer of the quantum-cutter couple Pr^{3+}–Mn^{2+} in CaF_2:Pr^{3+},Mn^{2+} nanoparticles. *J. Lumin.*, 2016, **179**, P. 555–561.

[21] Meijerink A., Wegh R., Vergeer P., Vlugt T. Photon management with lanthanides. *Opt. Mater.*, 2006, **28**, P. 575–581.

[22] Pudovkin M.S., Morozov O.A., Pavlov V.V., Korableva S.L., Lukinova E.V., Osin Y.N., Evtugyn V.G., Safiullin R.A., Semashko V.V. Physical Background for Luminescence Thermometry Sensors Based on Pr^{3+}:LaF_3 Crystalline Particles. *J. Nanomaterials*, 2017, Article No 3108586.